J Mater Sci (2008) 43:3522–3530
DOI 10.1007/s10853-008-2522-4

Microstructure development in Nb_3Sn(Ti) internal tin superconducting wire

I. Pong · S. C. Hopkins · X. Fu · B. A. Glowacki · J. A. Elliott · A. Baldini

Received: 13 August 2007 / Accepted: 31 January 2008 / Published online: 11 March 2008

Abstract The authors have studied the phase formation sequences in a Nb_3Sn 'internal tin' process superconductor. Heat treatments were performed to convert the starting materials of tin, Ti–Sn, copper and niobium, to bronze and Nb_3Sn. Specimens were quenched at different points of the heat treatment, followed by metallography to identify the phases present and X-ray microtomography (XMT) to investigate the void volume and distribution. An unexpected observation of the microstructure development was the uphill diffusion of tin during the Cu–Sn reactive diffusion. Some defects likely to affect the superconducting performance of the wires were observed. Microscopy revealed the presence of a Ti–Sn intermetallic compound displacing the niobium filaments, and XMT revealed the formation of long pores in the longitudinal direction. Two types of pore formation mechanism, in addition to Kirkendall pores, are proposed. The phase and microstructure development suggests that low-temperature heat treatment (below 415 °C) will have significant influence on optimising the final superconducting properties.

Introduction

Nb_3Sn superconductors are gaining market share in high magnetic field applications such as superconducting magnets for NMR, particle accelerators and plasma confinement in fusion applications. High critical current density and high upper critical field are essential for these applications and, to maximise these properties, good microstructure and stoichiometry controls are necessary. Currently there are three major ways of manufacturing wires: the internal tin [1], powder-in-tube (PIT) [2] and bronze processes [3].

In this study, two commercially produced internal tin wires (Outokumpu Copper) were investigated, hereinafter referred to as the 26-bundle and 85-bundle wires. The internal tin process starts with elemental niobium filaments and a tin core (with titanium as ternary addition) in a copper matrix surrounded by a tantalum–niobium diffusion barrier, forming 'bundles' (Table 1). A number of bundles distributed in concentric rings in a pure copper matrix constitute the wire (Fig. 1). The soft starting metals allow extrusion, swaging and drawing to the final diameter without the need for multiple anneals as would be required in the bronze process. After final deformation the wires undergo a multi-stage heat treatment, in which tin diffuses through copper, forming some of the Cu–Sn phases, and finally forming the superconducting A15-phase Nb_3Sn by reactive diffusion into the niobium filaments.

Titanium was added to the tin core in the wires investigated to facilitate wire drawing, increase Nb_3Sn layer growth rate and improve J_c at high magnetic fields [4, 5]. In the wires as received, the core contained a mixture of pure tin and the tin-rich intermetallic compound Ti_6Sn_5. It has been suggested [6, 7] that titanium increases Nb_3Sn formation rate by refining its grain size, whereby a higher grain boundary density accelerates tin diffusion through Nb_3Sn to Nb_3Sn/Nb interface; that the finer Nb_3Sn leads to higher J_c by virtue of increased number of pinning centres; and that higher H_{c2}, and consequently higher J_c at high

I. Pong (✉) · S. C. Hopkins · X. Fu · B. A. Glowacki · J. A. Elliott
Department of Materials Science and Metallurgy, University of Cambridge, Pembroke Street, Cambridge CB2 3QZ, UK
e-mail: ip241@cam.ac.uk

A. Baldini
Outokumpu Copper Superconductors, Via Della Repubblica 257, 55052 Fornaci Di Barga, Italy

Table 1 Composition of the 'bundles' in both wires

Composition (%)	Cu (%)	Nb (%)	Sn (%)	Ti
vol	57	25	18	Negligible
at	70	20	10	Negligible
wt	60	25	15	Negligible

Table 2 Proposed reaction scheme in Cu–Sn–Ti by Naka [9]. Note that the reaction temperatures here are the averages of several measurements

572 °C	$Ti_6Sn_5 + \varepsilon \leftrightarrows L + CuSnTi$
407 °C	$Ti_6Sn_5 + \eta \leftrightarrows L + \varepsilon$
227 °C	$Ti_6Sn_5 + Sn + \eta \leftrightarrows L$

field, arises due to the improved stoichiometry of Nb_3Sn resulting from the higher diffusion rate of tin in Nb_3Sn grain boundaries.

In addition, it has been reported that titanium appears to enhance formation of η and ε phases during tin mixing [4]. Nevertheless, it was suggested that the tin core should not have more than 4.8 at% Ti because of degradation of workability due to Ti_6Sn_5 [8].

Ti_6Sn_5 is a line compound that melts at 1,490 °C and has a phase transformation at 790 °C, which are above any temperature encountered during our heat treatment schedules. However, it is possible that two ternary invariant reactions occurred at around 223–230 °C and 405–412 °C, as suggested by Naka [9] (Table 2). The existence of these reactions was, however, uncertain, because the volume fraction of Ti_6Sn_5 present in our wires was small, and the reaction temperatures are too close to the melting points of tin and of η phase, for the reactions to be detected by differential scanning calorimetry or resistometry.

Defects and porosity formed in the bundles during manufacturing and reactive diffusion can degrade mechanical properties and, more importantly, can obstruct the diffusion paths of tin to niobium, resulting in tin-deficient Nb_3Sn and hence poor superconducting properties [10]. The connection between phase development and defect formation during heat treatment, and how the latter might be discouraged have been investigated.

Experimental method

Heat treatments were performed on wire samples ~100-mm long, encapsulated in quartz tubes under vacuum, in a box furnace controlled by a proportional integral time differential (PID) Eurotherm temperature controller. Samples reported here were not sealed at the ends, and some tin loss has been observed, but outer 10–20 mm lengths were discarded.

Two heat treatment schedules were provided, by Outokumpu and EFDA (European Fusion Development Agreement), and will be referred to as HT1 and HT2, respectively. The temperature profiles are shown in Fig. 2.

Heat treatment

Both the heat treatment schedules have five stages.

The two lowest-temperature steps (185–210 °C; 340–360 °C) are in the vicinity of the η/η' phase transition (187 °C) and of the δ phase formation (350 °C), according to Cu–Sn equilibrium binary phase diagram [11]. The purpose of these two steps is to convert tin (m.p. 231 °C) and η (m.p. 415 °C) to higher-melting phases. Ideally the conversion should be complete before the temperature is raised, to avoid the formation of liquid phases which would result in pressure build up, niobium filament movement and local loss of tin.

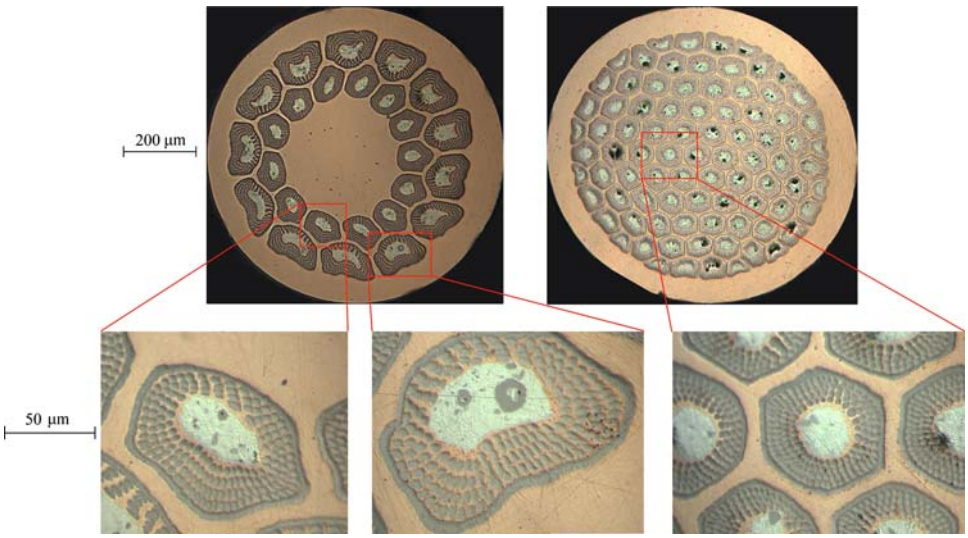

Fig. 1 Optical micrographs of the cross-sections of the two internal tin wires investigated. The bundles all came from the same production but were reduced by different ratios in the inner and outer rings of the 26-bundle wire (left) and in the 85-bundle wire (right). The voids observed in the 85-bundle wire above were sample preparation artefacts, where the hard Ti_6Sn_5 were ripped from the soft tin core during polishing

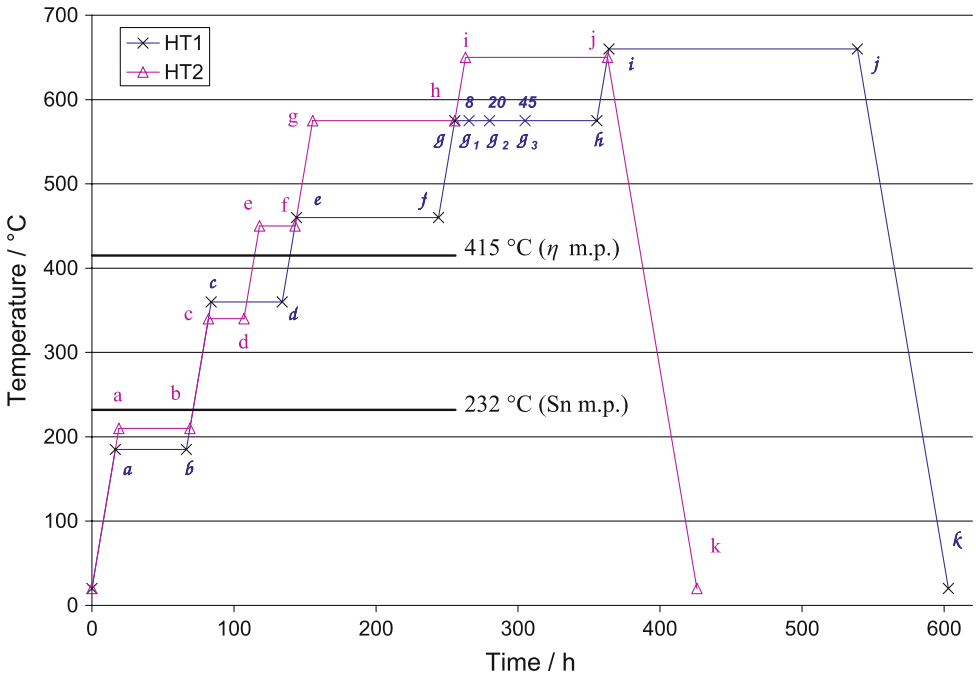

Fig. 2 Heat treatment schedules HT1 and HT2. All heating rates are 10 °C/h. Also indicated on the graphs are the melting points (m.p.) of pure tin and the tin-rich intermetallic compound Cu_6Sn_5 (η phase). Small letters indicate the points where specimens were quenched

As the heat treatment proceeds, progressively more copper-rich phases (ε, δ…α) are formed, the last of which is known to promote the formation of Nb_3Sn at a lower temperature [12]. From differential thermal analysis [13] and resistometry [14] it is known that the Nb_3Sn formation starts at about 530–550 °C (temperatures as low as 450 °C have been reported [12]), but the chief purpose of the intermediate steps (450–460 °C; 575 °C) is to convert ε and δ to α phase only. Industrially it also serves to remove organic contaminants [15].

The final step (650–660 °C) is designed to convert all niobium to Nb_3Sn and promote long range order. It is desirable to have a fine microstructure—in order to have more grain boundaries for better flux pinning and thereby higher J_c—and therefore this modest temperature is preferred to avoid excessive grain growth.

Examination techniques

Optical microscopy and scanning electron microscopy with energy dispersive X-ray spectroscopy (EDS) have been used to analyse the phase distribution, and composition and microstructure development. Scanning Electron Microscopes with thermionic (SEM) and field emission (FEGSEM) electron sources were used for EDS analysis, and secondary and backscattered electron imaging.

XMT is a non-destructive imaging and characterisation technique that can produce 3D images of materials with a voxel (volume picture element) size of the order of 1 μm^3, allowing the resolution of microstructural and compositional features associated with different X-ray absorbencies. It has been applied successfully in a number of fields within materials science and engineering including metal matrix composites [16], but only recently has it been applied, by Scheuerlein et al. [17, 18] and Pong et al. [14] independently, to superconducting wires.

A SkyScan-1072 desktop XMT system, which offers a maximum spatial resolution of the order of several micrometres, has been used to obtain tomographs of 1.8-mm length of the sample wires to investigate the pore volume and distribution.

Results and discussion

Titanium addition

Niobium filament displacement and distortion were observed in both as-received and reacted wires. Some were clearly caused by the hard intermetallic compound during wire manufacture (Fig. 3a, b). The Ti content in Sn is 4.8 at%, and the defect substantiates the suggestion [8] that a tin core with over 4.8 at% Ti should be avoided.

This intermetallic compound is observed in the as-received wire, during the low-temperature heat treatment and until the end of the dwell at 450–460 °C but not after ramping to 575 °C and beyond. It is observed to be disappearing as the heat treatment progressed (see Fig. 3a–g), and it is plausible that titanium diffuses towards the niobium filament alongside tin, and its dissolution and diffusion rates increase rapidly between these two temperatures. Also possible is that there are Cu–Sn–Ti ternary

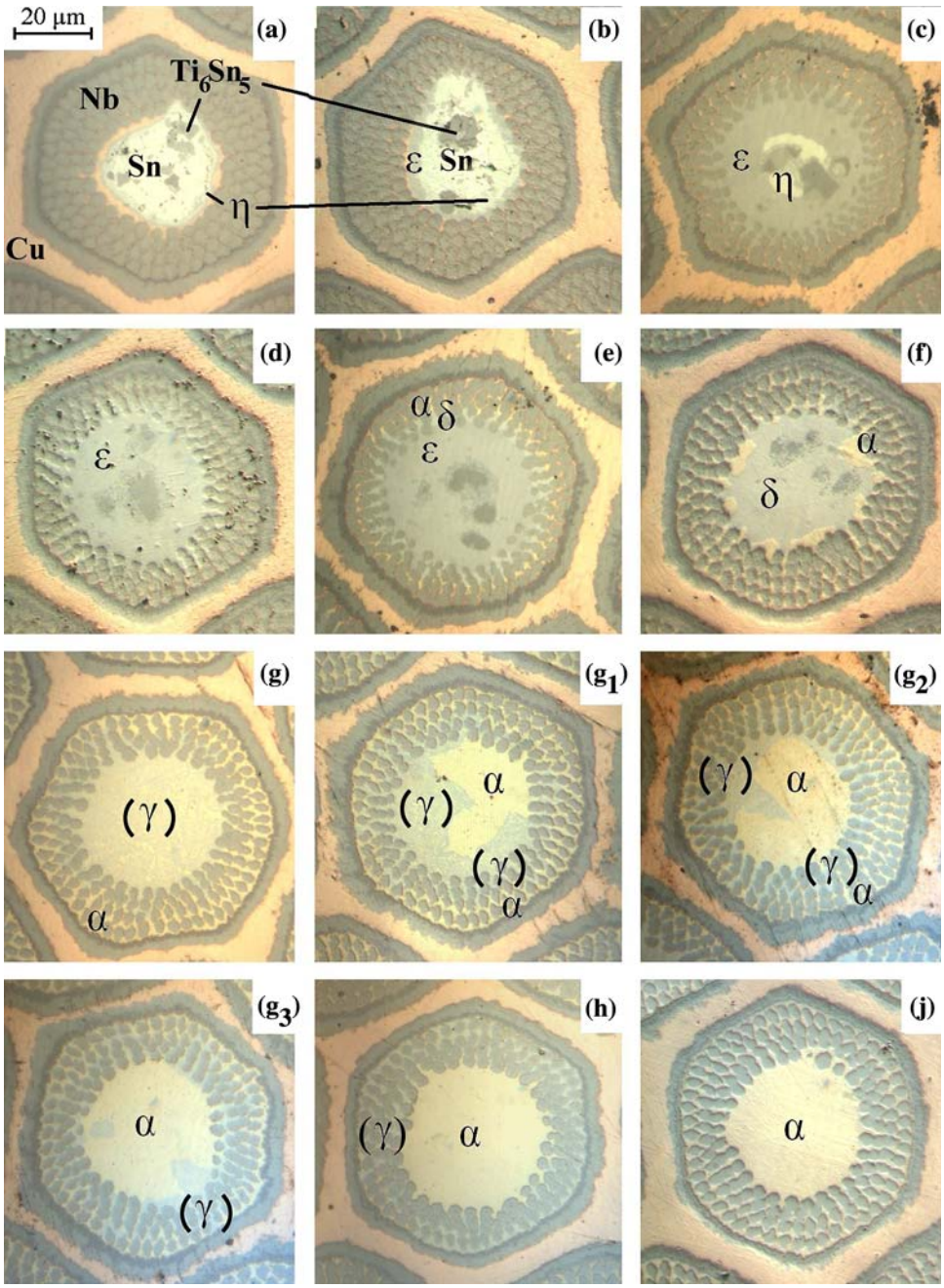

Fig. 3 Optical micrographs of bundles from the 85-bundle wire during HT1. Labels on top right corner indicate the stage from which the specimen was quenched, as marked in Fig. 2. Bracketed phases are believed to have existed at the reaction temperature but to have undergone eutectoid decomposition during cooling. Notice that in (**c**) the diffusion barrier was broken. Although this is very rarely observed, it would result in loss of tin from the bundle to the stabilising matrix, hence incomplete Nb_3Sn reaction and poorer stability. Also notice the concentration inversion between stages **g** and **h**

reactions, as suggested by Naka [9], such that at about 566–574 °C, Ti_6Sn_5 reacts with ε to form CuSnTi and a liquid phase (see Table 2 above): the chemical reaction and the formation of a liquid phase would greatly accelerate the dissolution of Ti_6Sn_5 and the diffusion of titanium.

At the end of the heat treatment, 1.0 ± 0.5 at% Ti is detected in Nb_3Sn filaments, but no detectable amount was observed in the bronze matrix (Fig. 4). Note that the filaments are twisted to minimise a.c. losses, and that the size of the interaction volume of the backscattered electrons is of the order of 1 μm, which may partly explain the detected copper, although it is also not impossible that copper has diffused into the filament.

The dissolution and diffusion of Ti were difficult to follow because Ti_6Sn_5 is not always distinguishable from δ and ε phases in optical microscopy, and from δ, ε, η/η′ and tin in the backscattered imaging mode of SEM. The fact that the hard intermetallic compound is embedded in a soft metal matrix makes it easily lost during sample preparation, and this artefact also affects the study of pore formation.

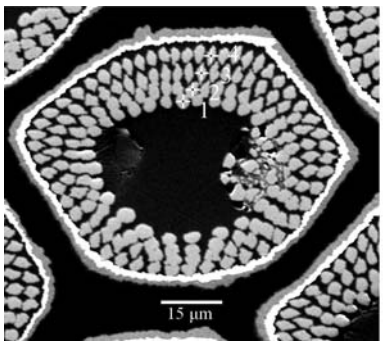

at %	Point 1	Point 2	Point 3	Point 4
Nb	70.4	71.6	71.7	70.8
Sn	22.4	21.7	21.5	22.2
Ti	0.6	0.6	0.6	0.5
Cu	6.5	6.1	6.0	6.2

Fig. 4 SEM backscattered electron image of a bundle from the 85-bundle wire at the end of HT2 with EDS results showing the composition of the filaments in at%. Note the broken niobium filaments in the bundle, which are believed to be defects produced during manufacture

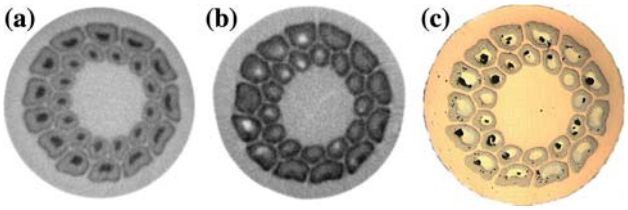

Fig. 5 XMT reconstructed 2D transverse cross-section images of (**a**) as-received wire, (**b**) after dwell at 575 °C, and (**c**) optical micrograph after dwell at 575 °C. Wire diameter is 0.8 mm

XMT and two types of pore formation

XMT is an effective technique for revealing and analysing pores non-destructively in three dimensions and has provided a more comprehensive picture of the nature of the pores formed particularly in the tin core than conventional metallography, although the phase contrast and spatial resolution in our machine were not sufficient to resolve individual niobium filaments or Ti_6Sn_5 (Fig. 5).

In studying porosity, especially pore interconnectivity, size and volume, conventional metallography could often give misleading results because what is seen in a 2D cross section is often not representative of the 3D structure. In the following XMT-reconstructed images (Figs. 6–8), sample wires as-received, heat treated to stage h (after dwell at 575 °C) and stage k (end of heat treatment) are presented, in 3D and 2D longitudinal cross section, showing the structure. It can be seen that depending on where the longitudinal cross section was taken, a 2D image could suggest fewer long pores in the sample after dwell at 575 °C than the one after full reaction, while a 3D image clearly shows otherwise!

New evidence provided by XMT also seems to suggest that, in addition to Kirkendall voids [19], there are two types of pores: those as a result of solid-phase transformation, and those of liquid-phase formation. The former are inevitable, as there is a density difference between different phases formed, most noteworthy being the shrinkage associated with the formation of the dense ε phase, and the 37% expansion upon formation of the

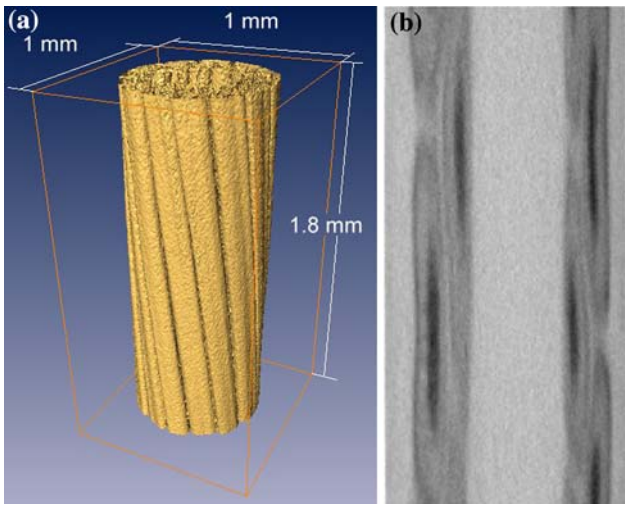

Fig. 6 As-received wire: (**a**) XMT-reconstructed 3D image, bundles only (pure copper matrix removed); and (**b**) XMT-reconstructed 2D longitudinal cross-section image, showing pure copper matrix (light grey), bundles and pure tin (black). Note that the bundles are twisted to minimise AC losses and therefore appear to be non-uniform in the 2D image

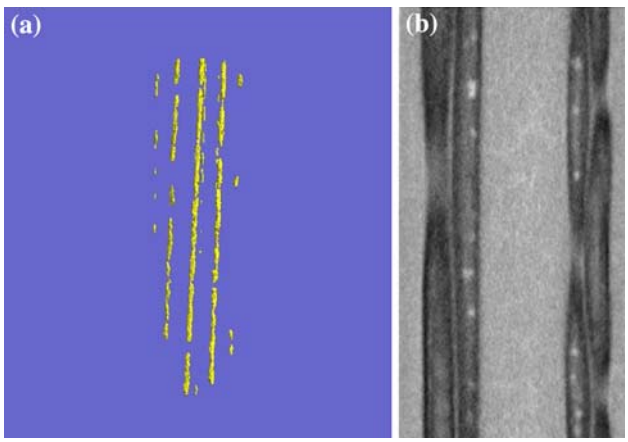

Fig. 7 After dwell at 575 °C: (**a**) XMT-reconstructed 3D image of pores only; and (**b**) XMT-reconstructed 2D longitudinal cross-section image, showing long pores (white)

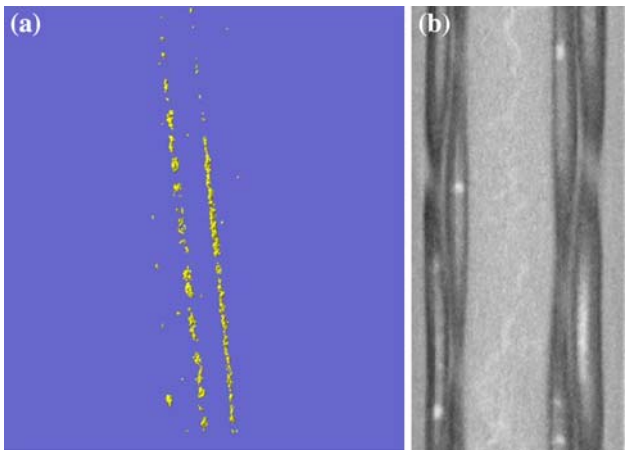

Fig. 8 After full reaction: (**a**) XMT-reconstructed 3D image of pores only; and (**b**) XMT-reconstructed 2D longitudinal cross-section image, showing long pores (white)

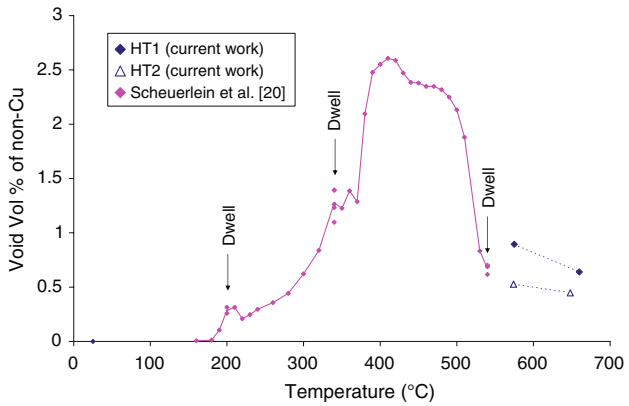

Fig. 9 Void volume (as percentage of non-Cu volume) as a function of heat treatment temperature. Note, however, that there are dwells (Scheuerlein et al. 200 °C, 340 °C, 540 °C; current work refer to Fig. 2) during which void volume develops, and that the ramp rates are 60 °C/h (Scheuerlein et al.) and 10 °C/h (current work)

superconducting A15-phase Nb_3Sn. It can be observed from the results of the elegant work done by Haibel and Scheuerlein et al. using synchrotron XMT to follow a single sample during a simplified heat treatment [20], that many of the pores formed during the solid-phase transformations will eventually be closed while those as a result of liquid-phase formation remain.

Our ex situ XMT results show long pores at the end of the 575 °C dwell and also at the end of the entire heat treatment, with a longer duration and a higher temperature than those investigated by Scheuerlein et al., who performed in situ synchrotron XMT during heat treatment [17, 18, 20], but both results, though using wires of different design, are in good agreement. All void volumes presented here were converted to percentages of the respective non-Cu volume for ease of comparison. The results show pore volume percentage of 0.895% (HT1, end of 575 °C dwell), 0.640% (HT1, end of reaction) and 0.528% (HT2, end of 575 °C dwell), 0.448% (HT2, end of reaction); compared to Scheuerlein's 2.61% at maximum void volume and 0.616–0.703% at 540 °C [20] (Fig. 9). The void volume is seen to decrease from 400 °C because the low-density δ is formed at the expense of the high-density ε. The void volume is expected to increase slightly again when α phase is formed from δ (in some cases, via γ). The void volume then falls back during the 650/660 °C dwell, due to the formation and associated volume expansion of Nb_3Sn. The morphology and amount of voids towards the end of the heat treatment closely resemble those at the point where liquid formation occurred (refer to Fig. 2 in [20] and Fig. 9 below).

Liquid-phase formation

The formation of liquid phases is undesirable because—apart from causing niobium filament movement and bridging—porosity and local depletion of tin are deemed to result in off-stoichiometric Nb_3Sn and hence degraded superconducting properties.

Microscopy showed that, with the present heat treatments, there was incomplete conversion of elemental tin, and of η phase, to higher-melting Cu–Sn intermetallics before ramping above their respective melting points. The formation of a liquid phase and the loss of tin is evident: large pores were observed in places where the low-melting phases were located, and at the end of the heat treatment the tin content of the α bronze matrix in bundles with such large pores believed to have been caused by loss of tin was found by EDS to be dramatically lower than that calculated and observed in bundles without such pores. According to stoichiometric calculations, the amount of Sn present in a bundle was sufficient to convert all Nb to Nb_3Sn and leave behind a 4 at% α bronze, and this was indeed observed in many bundles. In the case where evidence suggested formation of liquid phase had occurred, we observed incomplete conversion of Nb and a 1 at% α bronze as a result of local loss of tin.

It can be argued that in very long wires with sealed ends, by conservation of mass, the formation of liquid tin will not affect the overall tin concentration, but merely lead to local tin loss and at the same time local tin accumulation elsewhere, the effect of which could be eliminated by diffusion. However, although inhomogeneity might be reduced by increasing the annealing time to compensate for increased diffusion distances, the problem is that this would result in grain coarsening and thereby reduced density of pinning centres. Differences in the time required for complete reaction in tin-deficient regions (for example next to long pores) and relatively tin-rich regions also mean the A15 morphology and stoichiometry will vary both radially and longitudinally. Furthermore, it has been

reported that the total volume of voids is similar in wires with and without liquid-phase formation [17]. This implies that longitudinal inhomogeneity is made more severe by long pores formed as a result of liquid-phase formation.

Combining the XMT results of our own and those of Scheuerlein's, and the microscopy and EDS results, we argue that pores formed as a result of liquid-phase formation will be more likely to remain till the end of the heat treatment and cause long-range tin inhomogeneity, while those as a result of the formation of the dense ε phase will eventually be largely closed by the expansion upon lower density phases and Nb_3Sn formation, and do not result in a redistribution of tin as the tin is retained locally in ε.

Although the current work has not included J_c measurement, which will be essential to confirm the argument, and will be performed at the earliest opportunity, we herein refer to a paper by Dietderich et al. [21], who have, using a different internal tin wire, reported that wires heat treated straight up to 700 °C showed substantial porosity in the core regions but wires that underwent 200 °C/200 h + 375 °C/33 h + 580 °C/218 h saw only a ring of porosity through the filament region in some but not all of the sub-elements, and the core region void free. In addition, the critical current densities in the latter are higher by 15–20%, more uniform along the wire length and less dependent on annealing duration at the highest temperature. It seems, therefore, desirable to have a longer low-temperature treatment or a design of wire that would encourage quicker conversion of the low melting phases.

Some recent work on similar—but not identical—wires has suggested that the superconducting properties are independent of the tin mixing treatments before the final annealing for Nb_3Sn formation [22]. The said work, nevertheless, admitted that formation of liquid phase could lead to pressure build up and thus compromise the integrity of wires.

Tin distribution

In the current study, it has been observed that in samples quenched just before and shortly after the temperature was increased above the β-phase formation temperature, there were very fine, eutectoid-like regions alongside α phase (see Figs. 3g and 10, respectively). EDS results showed that the overall compositions of the eutectoid regions were 16.4 ± 0.5 at% Sn and 14.8 ± 0.5 at% Sn, in agreement with the eutectoid compositions of γ (16.5 at% Sn) and of β (14.9 at% Sn), respectively. In an attempt to identify the individual phases in these regions, FEGSEM EDS was performed with a low acceleration voltage of 7 kV to minimise the interaction volume. Quantification of point spectra gave average compositions of 17.42 at% Sn and 10.29 at% Sn for the two eutectoid components, suggesting

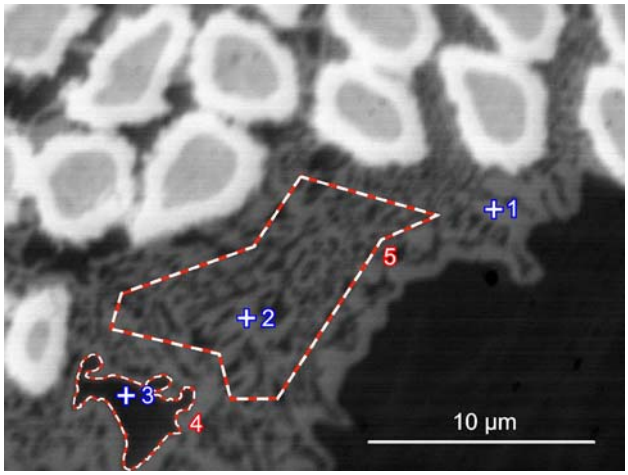

Fig. 10 FEGSEM backscattered electron image of a sample quenched from 3.5 h at 650 °C after the 575 °C dwell in HT1, above the β formation temperature. EDS was performed with a low acceleration voltage of 7 kV to minimise the interaction volume. Quantification of the spectra at points 1 and 2 gave compositions of 17.07 and 17.77 at% Sn, respectively, clearly above the eutectoid γ composition (16.5 at% Sn), suggesting it is δ with some stray signals from α nearby. Spectra from point 3 and region 4 gave compositions of 9.4 at% Sn and 10.98 at% Sn, respectively, suggesting they are α with some stray signals from δ nearby. The composition in region 5 was found to be 14.83 at% Sn, indicating it is very likely to have been β before quenching, whose eutectoid composition is 14.9 at%

that they are likely to be δ and α phases, respectively, with some stray signals from adjacent phases (Fig. 10).

Theoretical and experimental evidence from the phase diagram, FEGSEM EDS, and phase contrast in FEGSEM BEI and optical microscopy all point clearly to the eutectoid decompositions of $\gamma \rightarrow \alpha + \delta$ and $\beta \rightarrow \alpha + \delta$ in samples quenched just before and shortly after the temperature was increased above the β phase formation temperature, and it is therefore likely that the eutectoid reaction $\alpha + \gamma \rightarrow \beta$ occurred when the samples were heated above the β formation temperature of ~586 °C.

Unfortunately X-ray diffraction could not be used to more definitively identify these phases because the major 2θ peaks of the phases in question are too close (<1°), considering their low volume fractions and the off-stoichiometric and strained condition. We also did not observe, as reported by Acharya [23] in samples formed from Cu–Sn melts, a microstructural difference between the two $\alpha + \delta$ regions formed from β ($\beta \rightarrow \alpha + (\alpha + \delta)$) and from γ ($\gamma \rightarrow \alpha + \delta$), respectively.

The tin concentration in the core was observed to fall continually from pure tin to η, ε, δ, γ, and possibly β, and finally α (refer to Fig. 3 above), whereas the region between the niobium filaments and the edge of the tin core which started as pure copper, became the most tin-rich η, then ε, δ, γ, and possibly β, and finally α. The copper between niobium filaments, depending on whether it lies

close to the tin core or the diffusion barrier, typically transforms from Cu to α and ε (gaining tin), and then δ, γ, possibly β, and finally α (losing tin). As the tin concentration at the centre of the bundle decreases monotonically throughout heat treatment, a driving force for outward tin diffusion (in the form of an activity gradient) must also remain throughout. Surprisingly, in both wires and with both heat treatments, after the long dwell at 575 °C the distribution of tin was far from homogeneous: compared to the initial condition, the tin gradient was inverted, with the highest tin concentrations between the niobium filaments (see Fig. 3g–h).

It is at this stage not certain what the driving force was for the tin to diffuse 'uphill'. A possible explanation would be an unnoticed component (titanium) which changes the chemical activity, as in the classic example of Fe–Si–C [24]; another reason could be a quasi-capillary effect caused by the niobium filaments; and a third possible contribution is from the crystallographic orientation of the copper.

In a crystallography study by Park et al. [25] on the evolution of annealing textures in drawn copper wires, the centre and intermediate regions were reported to have strong fibre texture, and near-surface regions a circular texture. The tracer diffusivity for Cu in β-Sn is anisotropic, being 500 times higher in the *c* direction than the *a* direction [26]. It is therefore plausible that a substantial gradient of diffusivity could arise from a rotation of preferred orientation in some Cu–Sn systems. It is, however, unknown whether a similar phenomenon applies for the distributions of phases found in internal tin wires.

α bronze is generally accepted to promote the formation of Nb_3Sn, and the activity of Sn increases with Sn concentration up to the α-phase solubility limit [12]. It has been reported by Suenaga et al. that Nb_3Sn growth in contact with β phase is slower, and results in a lower critical current density, than in contact with α phase [27]; the same authors more tentatively proposed that the activity of tin in β phase is comparable to that just below the α-phase solubility limit. It might therefore be preferable to avoid β-phase formation by extending the reaction time below 586 °C, so that it cannot be formed at the expense of α phase.

The inversion of the composition profile may, however, be desirable, especially if it is retained when the phase between the niobium filaments is α. Under these conditions, it would encourage tin supply to the niobium interface and maximise the tin concentration at the interface, supporting the rapid growth of stoichiometric Nb_3Sn. It is therefore technologically as well as scientifically valuable to understand the mechanism behind this phenomenon.

In the 26-bundle wire it was observed that the tin mixing reaction and Nb_3Sn formation in larger outer-ring bundles, compared to those in smaller inner-ring bundles, are not always complete, presumably because the different bundle sizes—and hence different diffusion distances—require different heat treatments. Therefore, a compromise between full reaction in large bundles and potential grain growth in small bundles must be made if bundle size or design in a wire is chosen not to be uniform.

Conclusions

The phase and microstructure development during heat treatment of two internal tin process wires have been investigated, using optical microscopy, scanning electron microscopy and X-ray microtomography. A Ti–Sn intermetallic compound, Ti_6Sn_5, believed to have caused niobium filament displacement and necking, is observed in the tin core of the as-received wire and is eventually dissolved between 450 °C and 575 °C. Its possible dissolution and reactive diffusion were discussed.

Two types of pore formation, in addition to Kirkendall pores, are proposed for internal tin wires: those as a result of solid-phase transformation, which do not adversely affect the tin distribution and are inevitable, and those as a result of liquid-phase formation, which cause redistribution of tin (local depletion and local accumulation elsewhere) and can and should be avoided. We therefore emphasise the importance of low-temperature heat treatment (below 415 °C) in preventing the formation of long pores and locally off-stoichiometric Nb_3Sn.

Also observed was the unexpected 'uphill' diffusion of tin towards the niobium filaments, resulting in a concentration inversion. Finally, the observed differences in the degree of completion of reaction indicate that a wire with bundles of different sizes is unlikely to simultaneously achieve full reaction and small Nb_3Sn grain size.

Acknowledgements Ian Pong would like to thank the Croucher Foundation, Hong Kong, and Simon Hopkins the EPSRC, for financial support.

References

1. Yoshizaki K, Taguchi O, Fujiwara F, Imaizumi M, Wakata M, Hashimoto Y, Wakamoto K, Yamada T, Satow T (1983) IEEE Trans Magn 19:1131
2. Fischer CM, Lee PJ, Larbalestier DC (2002) In: Advances in cryogenic engineering, vols 48a and b; vol 614, p 1008
3. Kaufmann AR, Pickett JJ (1971) J Appl Phys 42:58
4. Suenaga M, Klamut CJ, Higuchi N, Kuroda T (1985) IEEE Trans Magn 21:305
5. Yoshizaki K, Wakata M, Miyashita S, Fujiwara F, Taguchi O, Imaizumi M, Hashimoto Y (1985) IEEE Trans Magn 21:301
6. Hayase T, Kajihara M (2006) Mater Sci Eng A 433:83

7. Osamura K, Ochiai S, Kondo S, Namatame M, Nosaki M (1986) J Mater Sci 21:1509
8. Miyashita S, Yoshizaki K, Hashimoto Y, Sekine H, Tachikawa K (1987) IEEE Trans Magn 23:629
9. Naka M, Schuster JC, Nakade I, Urai S (2001) J Phase Equilib 22:352
10. Godeke A (2005) Performance Boundaries in Nb3Sn Superconductors. PrintPartners Ipskamp, Enschede. ISBN 90-365-2224-2
11. Raynor GV (1944) Annotated equilibrium diagram series: No 2. The Institute of Metals, London
12. Lefranc G, Muller A (1976) J Less-Common Met 45:339
13. Tan KS (2006) PhD Thesis, University of Cambridge
14. Pong I, Hopkins SC, Fu X, Glowacki BA, Elliott JA, Baldini A (2006) Defect Diffus Forum 258–260:294
15. Muller M, Schulz H, Kirchmayr H (2005) Physica C 419:115
16. Watson IG, Lee PD, Dashwood RJ, Young P (2006) Metall Mater Trans A 37A:551
17. Haibel A, Scheuerlein C (2007) IEEE Trans Appl Superconduct 17:34
18. Scheuerlein C, Oberli L, Michiel D, Reichert K (2006) Voids in Nb_3Sn strands observed by synchrotron absorption microtomography. Poster presented at the International Cryogenic Materials Conference, 17–21 July 2006, Prague, Czech Republic
19. Easton DS, Kroeger DM (1979) IEEE Trans Magn 15:178
20. Scheuerlein C, Di Michiel M, Haibel A (2007) Appl Phys Lett 90:132510
21. Dietderich DR, Glazer J, Lea C, Hassenzahl WV, Morris JW (1985) IEEE Trans Magn 21:297
22. Naus MT, Jewell MC, Lee PJ, Larbalestier DC (2002) In: Advances in cryogenic engineering, AIP conference proceedings, vols 48a and b; vol 614. Amer Inst Physics, Melville, NY, ISBN 0-7354-0060-1, p 1016
23. Acharya NN (2001) J Mater Sci 36:4779
24. Darken LS (1949) Trans Am Inst Minerals 180:430
25. Park H, Lee DN (2003) Metall Mater Trans A 34:531
26. Dyson BF, Anthony TR, Turnbull D (1967) J Appl Phys 38:3408
27. Suenaga M, Horigami O, Luhman TS (1974) Appl Phys Lett 25:624